ACS OMEGA

http://pubs.acs.org/journal/acsodf

Article

Room Temperature Ca^{2+}-Initiated Free Radical Polymerization for the Preparation of Conductive, Adhesive, Anti-freezing and UV-Blocking Hydrogels for Monitoring Human Movement

Hui Lv, Shiyu Zong, Tong Li, Qian Zhao, Zhiyong Xu, and Jiufang Duan*

Cite This: *ACS Omega* 2023, 8, 9434−9444

Read Online

ACCESS | Metrics & More | Article Recommendations | Supporting Information

ABSTRACT: In recent years, conductive hydrogels have received increasing attention as wearable electronics due to the electrochemical properties of conductive polymers combined with the softness of hydrogels. However, conventional hydrogels are complicated to prepare, require high temperature or UV radiation to trigger monomer polymerization, and are frozen at low temperatures, which seriously hinder the application of flexible wearable devices. In this paper, a conductive sensor integrating mechanical properties, adhesion, UV shielding, anti-dehydration, and anti-freeze was prepared based on Ca^{2+}-initiated radical polymerization at room temperature using the synergy of sodium lignosulfonate, acrylamide (AM), and calcium chloride ($CaCl_2$). Metal ions can activate ammonium persulfate to generate free radicals that allow rapid gelation of AM monomers at room temperature without external stimuli. Due to ionic cross-linking and non-covalent interaction, the hydrogels have good tensile properties (1153% elongation and 168 kPa tensile strength), high toughness (758 $KJ{\cdot}m^{-3}$), excellent adhesive properties (48.5 kPa), high ionic conductivity (7.2 $mS{\cdot}cm^{-1}$), and UV resistance (94.4%). $CaCl_2$ can inhibit ice nucleation, so that the hydrogels have anti-dehydration and frost resistance properties and even at −80 °C can maintain flexibility, high conductivity, and adhesion. Assembled into a flexible sensor, it can sense various large and small movements such as compression, bending, and talking, which is a flexible sensing material with wide application prospects.

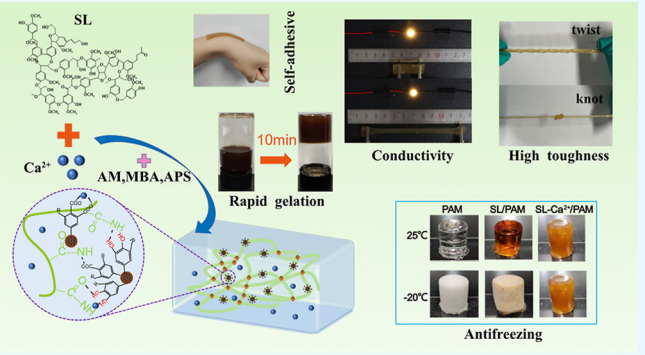

1. INTRODUCTION

As a promising material, conductive hydrogels have attracted extensive attention in the fields of flexible wearable sensor, flexible supercapacitor,[1,2] ionic skin,[3] friction nano-generator coating,[4,5] and so on. Conductive hydrogels can be divided into electronic conductive hydrogels and ionic conductive hydrogels according to the different transmission media.[3] The former is doped with conductive fillers such as carbon nanotubes,[6,7] silver nanowires,[7,8] graphenes (GO),[9−11] MXenes,[12,13] polypyrrole,[14] etc. The latter uses soluble metal salt ions such as Al^{3+}, Zn^{2+}, Fe^{3+}, Na^{+}, Ca^{2+}, K^{+}, etc.[15] Efforts have been taken to develop conductive hydrogels with good properties, but the poor mechanical strength, tedious preparation process, and adhesion to other materials limit their practical applications.

To avoid the effect of using additional binders on the conductivity of hydrogels, there is an increasing demand for conductive hydrogels with biocompatible and adhesive properties for flexible sensors, electronic skins, and conductive coatings. In recent years, research on adhesive hydrogels has focused on biomimetic mussels,[16] polysaccharides,[17,18] protein stickiness,[19] and base pair.[20,21] Self-adhesive properties of hydrogels are conferred by non-covalent bonding interactions between specific functional groups in the hydrogel and the surface of the object, such as hydrogen bonding, metal−ligand complexes, $\pi-\pi$ stacking, hydrophobic interaction, and so on.[22,23] Thanks to the superb adhesion of marine mussels to various substrates,[24] the preparation of adhesive hydrogels based on catechol compounds,[25,26] such as polydopamine, lignin, and tannins, has become a research hotspot recently. Due to the catechol groups contained in the hydrogels, the covalent and non-covalent interactions on various substrates confer self-adhesive properties. Lignin, as the second most abundant natural polymer after cellulose, contains hydroxyl, methoxy, and carboxyl groups with properties such as antioxidant, antibacterial, UV shielding, low degradation, high strength, and high yield,[27−29] which make it a good choice for the preparation of hydrogels as components containing catechol groups.

Received: December 20, 2022
Accepted: February 23, 2023
Published: March 3, 2023

In addition, most hydrogels cannot be used in extreme environments, such as low temperatures. Low temperatures can make the hydrogels freeze. Even at ambient temperatures, hydrogels dry out and harden due to water evaporation, which severely weakens the properties of hydrogels,[30] such as flexibility, electrical conductivity, and tensile properties, hindering their long-term usability. Therefore, it is a challenge to design a hydrogel that is frost resistant, has moisture retention properties, and can be used for a long time. $CaCl_2$ is widely used to prevent ice formation on roads or house construction. Relying on the physicochemical properties of $CaCl_2$, it lowers the freezing point of water,[31−33] thus imparting anti-freeze and anti-dehydration properties to hydrogels.

The preparation process of conventional hydrogels requires high temperature or UV initiation, or the introduction of toxic catalysts, which makes the preparation process tedious. Therefore, it is of great significance to develop hydrogels with excellent properties and simple preparation. It has been demonstrated that metal ions can activate persulfate to form free radicals through the electron transfer process[23,32,34] and can autocatalyze the gelation of hydrogels at room temperature or low temperature without the help of external stimuli. In this study, SL-Ca^{2+}/PAM hydrogels were prepared by a simple one-step method by co-blending SL, AM, and $CaCl_2$. Ca^{2+} activated the APS to produce $SO_4^{-\bullet}$ through the electron transfer process, triggering the polymerization of AM monomers within minutes at room temperature without UV radiation or high temperature initiation, while imparting electrical conductivity and antifreeze properties to the hydrogel. SL has good water solubility and contains functional groups such as benzene ring, phenolic hydroxyl group, carbonyl group, and carboxyl group to give hydrogel adhesion and UV resistance. Furthermore, Ca^{2+} also forms metal ion coordination bonds with carboxyl groups and catechol groups on SL, which act as sacrificial bonds,[35,36] effectively dissipating energy and enhancing mechanical properties. In conclusion, we obtained the SL-Ca^{2+}/PAM hydrogel, which combines many properties of anti-freezing, moisture retention, good mechanical properties, high electrical conductivity, long-term stable adhesion, and UV shielding by a simple process. It was assembled into a flexible sensor that can sense various large and small movements such as compression, bending, and talking, making it a flexible sensing material with wide application prospects.

2. EXPERIMENTAL SECTION

2.1. Materials. Sodium lignosulfonate (SL) was provided by Shandong Ruijiang Chemical Industry Co., Ltd. Acrylamide (AM) was purchased from Macklin Industrial Corporation (Shanghai, China). *N*, *N*′-methylene bisacrylamide (MBA) was purchased from Shanghai Yien Chemical Technology Co., Ltd. Ammonium persulfate (APS) was purchased from Xilong Chemical Co., Ltd. Calcium chloride anhydrous ($CaCl_2$) was supplied by Aladdin Reagent Company Limited (Shanghai, China). All the chemicals were analytically pure grade and were used as received without further purification.

2.2. Preparation of the SL-Ca^{2+} Precursor. First, 30 mg of SL was added into 5 g of deionized water and stirred evenly. Then, 4 g $CaCl_2$ was added and stirred with a magnetic stirrer for 2 h at room temperature. Lastly, ultrasonic treatment was carried out to remove bubbles and foams. The SL-Ca^{2+} precursor was obtained.

2.3. Preparation of SL-Ca^{2+}/PAM Hydrogels. SL-Ca^{2+}/PAM hydrogels were prepared by the one-pot method at room temperature without external stimulation. In detail, 2 g AM was added to 3 g deionized water, followed by 2 mg MBA and 40 mg APS, then stirred at room temperature for 40 min until all the chemicals dissolved to form a homogeneous mixture solution. After that, the SL-Ca^{2+} precursor was added into the mixture solution and stirred for a few minutes to form SL-Ca^{2+}/PAM hydrogels. The detailed compositions of SL-Ca^{2+}/PAM hydrogels are shown in Tables S1−S4.

2.4. Spectroscopic and Morphological Analysis. Fourier transform infrared (FTIR) spectroscopy of the samples was obtained using a Tensor 27 FTIR spectrometer (Tensor 27, Nicolet Brooke Company, Germany) within the frequency range 400−4000 cm^{-1}.

The oxidation products of SL and reduction products of Ca^{2+} were measured using X-ray photoelectron spectroscopy (XPS) (K-Alpha$^+$, Thermo Scientific, USA) with monochromatic Al Kα X-ray (HV = 1486.6 eV) operated at 15 kV and 5 mA. All binding energies were referenced to the neutral C 1s peak at 284.6 eV to compensate for surface charging effects.

The morphology of the composite hydrogel was observed by scanning electron microscopy (SEM) (SU8010, Hitachi, Japan). The samples were freeze-dried to completely remove moisture from the hydrogel network. Then, the freeze-dried section sprayed with gold was observed by a scanning electron microscope under an acceleration voltage of 6 kV.

2.5. Mechanical Tests. The mechanical properties of hydrogels were tested using a Universal testing machine (UTM2203HA, SUNS Corporation, China). In the tensile tests, the 100 N sensor was used, the tensile rate of all experiments was controlled at 150 mm·min^{-1}, and the hydrogels were cut into a dumbbell shape with a length of 75 mm, a width of 4 mm, and a thickness of 2 mm. In the cyclic tensile tests, the hydrogels were stretched to a certain strain at a speed of 150 mm·min^{-1} and then unloaded immediately at the same speed without waiting. Young's modulus was calculated from the slope of the initial linear region of the stress−strain curve (5−15% strain). The toughness was estimated from the area under the stress−strain curve, and the dissipated energy was calculated from the area between the loading−unloading curve. During the compression tests, a 2000 N sensor was used, the compression rate of all experiments was controlled at 5 mm·min^{-1}, and the hydrogel samples were made into a cylinder with a diameter of 17.5 mm and a height of 20 mm. Similarly, in the cyclic compression tests, the hydrogel samples were compressed to a certain strain at 5 mm·min^{-1} and then unloaded immediately at the same speed without waiting. For testing the mechanical properties of the hydrogels at low temperatures, the dumbbell-shaped hydrogels were placed at 0, −20, and −80 °C for over 24 h. Then, these samples immediately examined when the hydrogels were taken out.

2.6. Adhesion Tests. The adhesive strength of hydrogels with glass, wood, stainless steel, and polydimethylsiloxane was measured by tensile adhesion tests. The hydrogel specimens were cut into 25 mm × 25 mm and pasted between the two same pieces for tensile adhesion tests. The tests were carried out using a universal testing machine with a 100 N sensor with a tensile speed of 5 mm·min^{-1}. The adhesive strength was calculated by dividing the measured maximum load by the adhesive area. For adhesion performance at low temperatures, the hydrogels were initially sandwiched between glass sheets

https://doi.org/10.1021/acsomega.2c08097
ACS Omega 2023, 8, 9434−9444

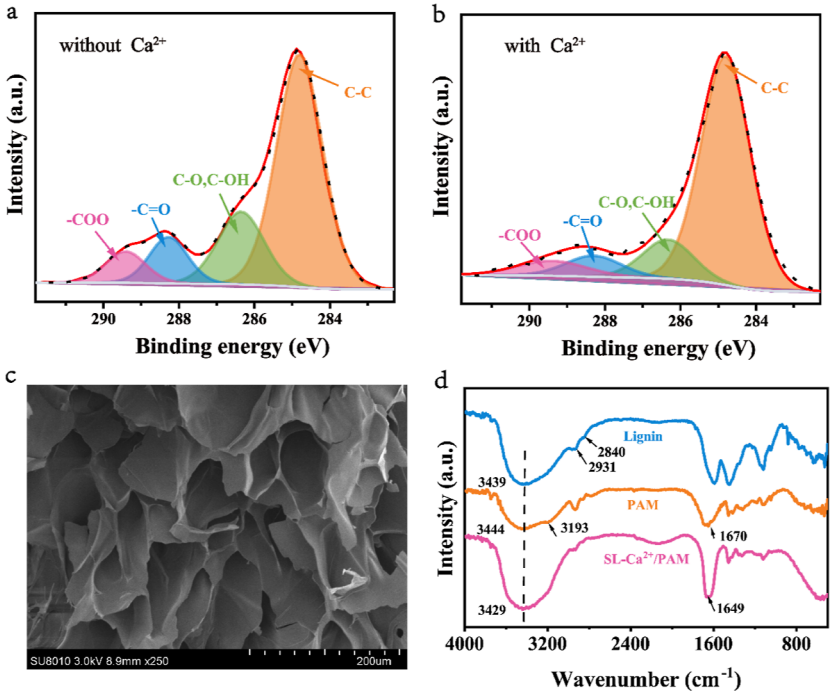

Figure 1. Characterizations of the SL-Ca^{2+}/PAM hydrogel. (a,b) High-resolution C 1s XPS for the SL and SL-Ca^{2+} suspensions, respectively; (c) SEM images of the freeze-dried SL-Ca^{2+}/PAM hydrogel; (d) FTIR spectra of SL, PAM hydrogel, and SL-Ca^{2+}/PAM hydrogel, respectively.

and then placed at 0, −20, and −80 °C for over 24 h. They were then removed for immediate testing.

2.7. Electrical Tests. The electrical conductivity (mS·cm^{-1}) of the hydrogels was tested by the electrochemical detector (800D, Shanghai Chenhua Instrument Co., Ltd., China). The conductivity of hydrogels at low temperatures was determined by placing the hydrogels at 0, −20, and −80 °C for 24 h. The formula was as follows

$$\sigma = \frac{L}{RS} \times 10^3 \quad (1)$$

where L (cm) is the distance between adjacent electrodes, R (Ω) is the hydrogel resistance measured by the electrochemical workstation at room temperature, and S (cm^2) is the cross-sectional area of the hydrogel. In addition, an electrochemical detector was also used to stretch the hydrogels to different strains and adhere to different parts of the human body under 0.1 V constant pressure. The resistance change rate of the hydrogel sample was obtained by measuring the resistance change of the hydrogel, namely

$$\Delta R/R_0 = \frac{R - R_0}{R_0} \times 100\% \quad (2)$$

where R_0 is the resistance in the initial state, and R is the real-time resistance under a certain strain. Meanwhile, the gauge factor (GF) was defined as

$$\mathrm{GF} = ((R - R_0)/R_0)/\varepsilon \quad (3)$$

where ε is the applied strain.

2.8. UV-Resistance Tests. The visible light and UV transmittance of hydrogels with a wavelength range of 800−200 nm were measured by a UV−vis spectrophotometer (T6 New-Century, Beijing Purkinje General Instrument Co., Ltd., China). Three hydrogel samples with a thickness of 2 mm were spread on one side of the cuvette for measurement.[37]

2.9. Anti-freezing Property Tests. The freezing point of hydrogels was measured by the differential scanning calorimetry (DSC) (Q2000, TA, USA) method to study their freezing resistance. DSC measured the temperature range from −80 to 50 °C with a constant cooling/heating rate of 5 °C·min^{-1}. In order to explore the moisture retention ability of the hydrogels, the hydrogels were placed in an environment with a temperature of about 30 °C and a relative humidity of about 80%, and the weight change was calculated by the following equation

$$\text{weight change } (\%) = \frac{w_t - w_0}{w_0} \times 100\% \quad (4)$$

where W_0 and W_t were the initial weight of the hydrogels and the weight of the hydrogels at time t, respectively.

3. RESULTS AND DISCUSSION

3.1. Design Rationale of the SL-Ca^{2+}/PAM Hydrogels. The preparation process of traditional hydrogels is complicated due to high temperature heating or long-time UV irradiation and other reasons.[38,39] In addition, the hydrogels produced have insufficient mechanical strength, weak bond performance, no resistance to low temperatures, no UV resistance, and so on, which hinder their practical application. In this study, an autocatalytic room temperature rapid gelation hydrogel was developed. By the simple and direct one-step rapid free radical polymerization of SL, AM, and $CaCl_2$, the hydrogels were prepared with excellent mechanical properties, adhesion, low temperature resistance, conductivity, and UV resistance. Metal ions were widely used as functional components. Metal ions can initiate free radical polymerization through the electron transfer process that reduces the activation energy of $S_2O_8^-$ homolysis to generate free radical $SO_4^{-\bullet}$ in monomer solutions,[40,41] to initiate monomer polymerization. No additional initiation conditions were required, such as high

https://doi.org/10.1021/acsomega.2c08097
ACS Omega 2023, 8, 9434−9444

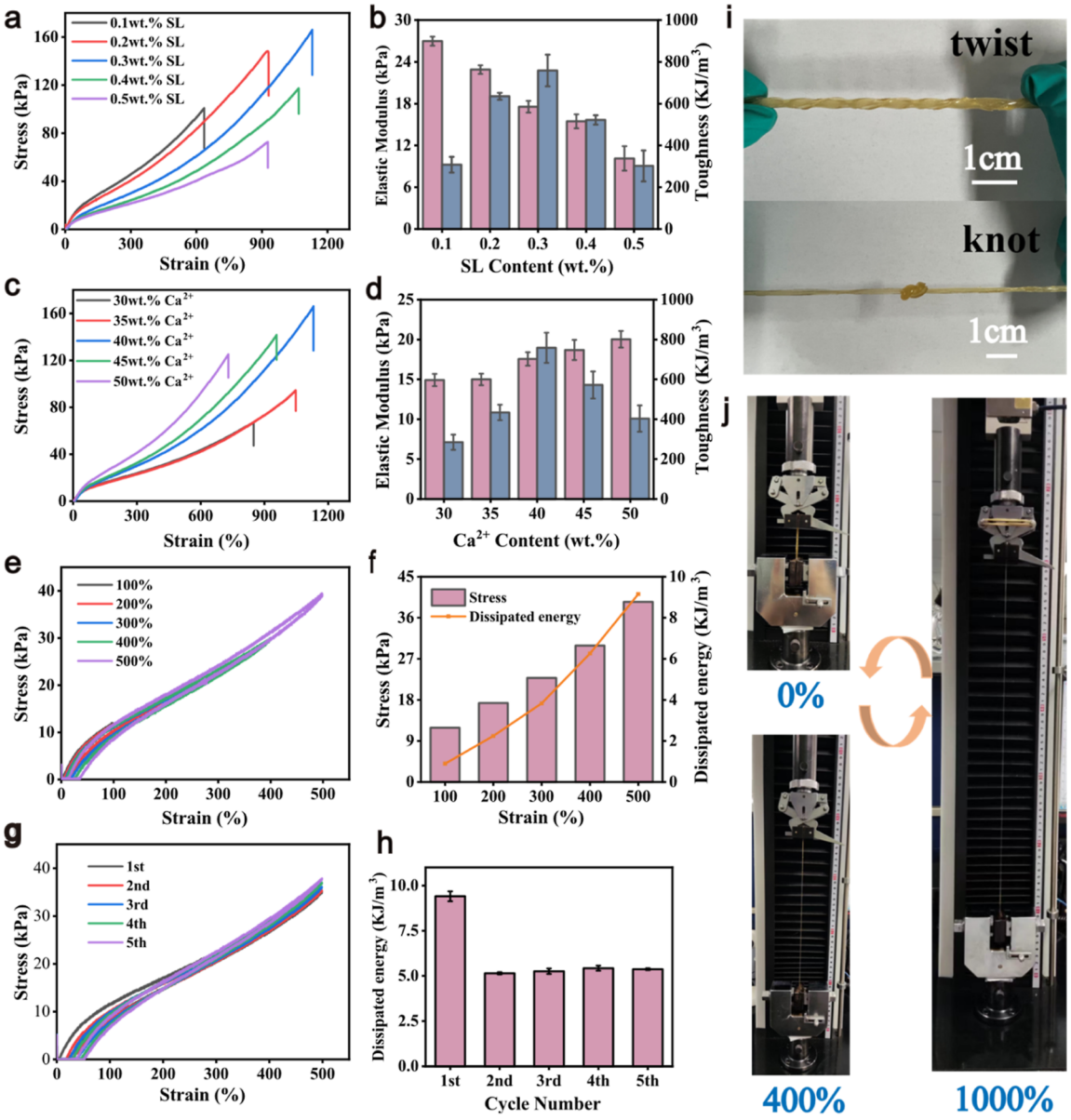

Figure 2. Tensile performance of SL-Ca^{2+}/PAM hydrogel. (a) Stress−strain curves of the hydrogels containing different amounts of SL; (b) corresponding elastic modulus and toughness of (a); (c) stress−strain curves of the hydrogels containing different amounts of Ca^{2+}; (d) corresponding elastic modulus and toughness of (b); (e) cyclic tensile curves of the SL-Ca^{2+}/PAM hydrogels with the predetermined strain increasing from 100 to 500%; (f) corresponding stress and dissipated energy of (e); (g) cyclic loading−unloading curves of the SL-Ca^{2+}/PAM hydrogels at 500% strain; (h) corresponding dissipated energy of (g); (i) deformations of the hydrogels, including twist and knot; (j) images of the hydrogels in tensile test.

temperature, UV radiation, etc. In addition, the hydroxyl and carboxyl groups in SL can form coordination sites with Ca^{2+},[35,36,42] giving the hydrogel tunable and enhanced mechanical properties. The coordination reaction of SL with Ca^{2+} was analyzed using XPS.[43,44] It can be seen from Figure 1a,b that the content of −C═O, C−O, C−OH, and −COOH decreased after the addition of Ca^{2+} to the SL solution, due to the dynamic ionic cross-linking between Ca^{2+} and the −OH and −COOH groups on SL. Figure 1d shows the FTIR spectra of SL, PAM hydrogel, and SL-Ca^{2+}/PAM hydrogel. The two peaks at 3444 and 3193 cm^{-1} in the PAM spectrum represent N−H asymmetrical stretching vibration and symmetric stretching vibration.[45] Compared to the native PAM hydrogel, the absorption peak of $-CO-NH_2$ in the SL-Ca^{2+}/PAM hydrogel shifted from 1670 to 1649 cm^{-1}, confirming that the long polyacrylamide chains were entangled with each other through hydrogen bonds and formed a strong interaction with SL.[46] The absorption peak at 2931 cm^{-1} in the spectra of SL was attributed to the stretching vibration of $-CH_3$ and $-CH_2$. The peak at 2840 cm^{-1} was $-OCH_3$ stretching. Obviously, the intensity of these peaks decreased or disappeared, indicating that $-OCH_3$ groups were consumed during SL oxidation.[47] The content of SL and $CaCl_2$ affected the gel speed, as shown in the Figure S5; the gelation time became longer as the SL content increased, in contrast to the gel formation time which became shorter with the increase of $CaCl_2$. This is due to the fact that the higher the $CaCl_2$ content, the easier it is to activate the APS to produce free radicals, which trigger the monomer polymerization at room temperature, and therefore the faster the gel formation speed. When the SL content

https://doi.org/10.1021/acsomega.2c08097
ACS Omega 2023, 8, 9434−9444

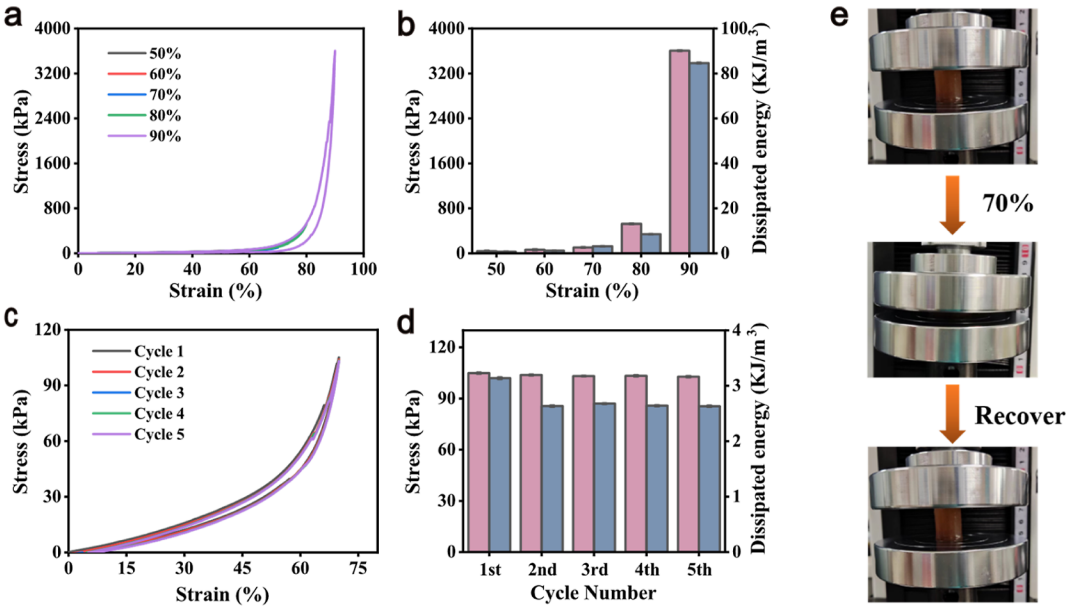

Figure 3. Compression performance of the SL-Ca^{2+}/PAM hydrogel. (a) Cyclic compression curves of the SL-Ca^{2+}/PAM hydrogel with the predetermined strain increasing from 50 to 90%; (b) corresponding stress and dissipated energy of (a); (c) cyclic loading−unloading curves of the SL-Ca^{2+}/PAM hydrogel at 70% strain; (d) corresponding dissipated energy of (c); (e) images of the hydrogels in compression test.

increases, the gelation speed slows down, which is possibly because the SL would scour free radicals to inhibit intermolecular cross-linking. It has been reported that salt lowers the freezing point of water by preventing it from forming a solid phase.[33,41,48,49] When $CaCl_2$ was added to the hydrogels, the spaces between the water molecules were filled with $CaCl_2$ particles, giving the hydrogels anti-freezing properties. Based on this design mechanism, we have obtained hydrogels with good mechanical properties, adhesion properties, frost resistance, and UV resistance, which have broad application prospects in the field of wearable sensors.

3.2. Mechanical Properties of the SL-Ca^{2+}/PAM Hydrogels. In order to prolong the service life of wearable sensors, hydrogels must have certain extensibility and toughness. SL-Ca^{2+}/PAM hydrogels can withstand mechanical deformation such as twisting and knotting to ensure the stability of wearable sensors (Figure 2i). The mechanical properties of SL-Ca^{2+}/PAM hydrogels were studied in detail in Figures 2 and 3. First, the effect of SL content on the mechanical properties of hydrogel was studied (Figure 2a,b). The $SL_{0.3wt\%}$ hydrogel was elastic and could withstand a tensile strain of up to 1153%. The addition of SL caused a decrease in the cross-linking density of the hydrogel, as evidenced by the consistent decrease in the modulus of elasticity. The hydrogel became softer and the strain increased, with a consequent improvement in the stress. However, too much SL caused the hydrogel to be too soft, and their stress and strain were reduced. This was because the complex polyphenol structure of SL deteriorates its mechanical properties.[40] It can be seen from Figure 2c,d that the content of Ca^{2+} in the system had a significant impact on the tensile properties of hydrogels. With the increase of Ca^{2+}, the cross-linking density increased and the tensile strain and elongation at break increased. But too much Ca^{2+} lead to excessive cross-linking and made the hydrogel brittle. Thus, both stress and strain again decreased. Figure S1a,b investigates the effects of monomer content and cross-linker dosage on the tensile properties of hydrogels. To sum up, when SL, AM, MBA, and Ca^{2+} were 0.3 wt %, 20 wt %, 0.1 wt % (MBA/AM) and 40 wt %, respectively, the breaking elongation and tensile stress were better, which was 1153% of breaking elongation and 168 kPa of breaking stress, and its toughness was also as high as 758 $KJ{\cdot}m^{-3}$. It is much higher than those of most of the lignin-based hydrogels reported in the literatures (Table S5). In order to better evaluate the properties of hydrogels, this formula hydrogel was selected as a typical sample for subsequent testing (the other tests were the same sample). Dissipation capacity[50] is a common standard to measure the durability of flexible sensors. Figure 2e−h shows the cyclic tensile test of hydrogels. When the maximum strain increased from 100 to 500%, an obvious hysteresis loop appeared (Figure 2e), indicating that the destruction and reconstruction of the hydrogen bond network in the hydrogel effectively dissipated energy.[19,23] Five consecutive load−unload cycles were performed at a constant 500% strain (Figure 2g). It was worth noting that the energy dissipated for the first time was large, and the energy dissipated for the next four times was almost stable, which reflected the excellent fatigue resistance of hydrogels. The same cyclic phenomenon was also reflected in compression. When the hydrogel was compressed to 90% strain, it can return to its original shape without obvious damage (Figure 3a), which reflected its good toughness and mechanical strength. Under 70% compression strain, there was a relatively large hysteresis loop for the first time. In the last four compression cycles, the hysteresis loops almost overlap (Figure 3c,d). The SEM image in Figure 1c confirmed the interwoven porous structure of SL-Ca^{2+}/PAM hydrogels, which dissipated energy through breaking and reforming dynamic hydrogen bonds and coordination bonds.[41] Figure S2 shows the uniform distribution of C, O, N, and Ca elements in hydrogels.

3.3. Self-Adhesive Properties of the SL-Ca^{2+}/PAM Hydrogel. The adhesive property of hydrogels is an important factor for wearable sensors. Mussel[16,51,52] is a natural marine organism, which can firmly adhere to the surface of many different materials in the sea. SL contains catechol groups and has mussel-like adhesive ability. SL-Ca^{2+}/PAM hydrogels can

https://doi.org/10.1021/acsomega.2c08097
ACS Omega 2023, 8, 9434−9444

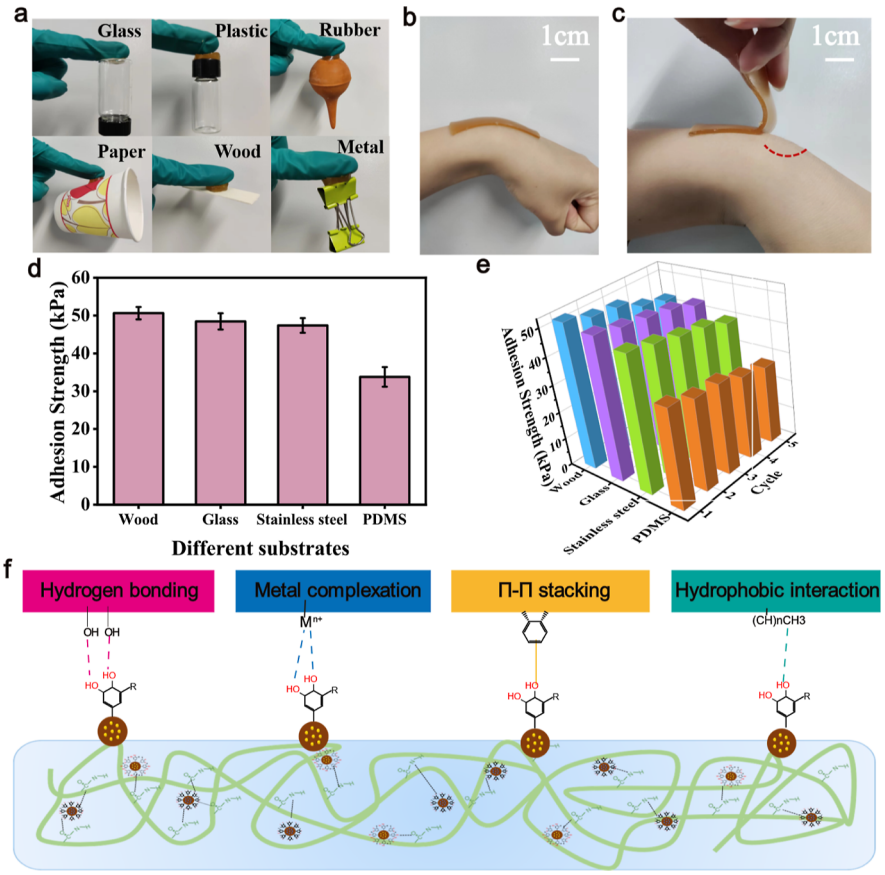

Figure 4. Adhesiveness of the SL-Ca^{2+}/PAM hydrogel. (a) Photographs of SL-Ca^{2+}/PAM hydrogels adhered to various substrates (glass, plastic, rubber, paper, wood, and metal); (b) Hydrogel adhering to human skin; (c) Hydrogel detaching from human skin; (d) adhesion strength of the hydrogels to various substrates; (e) repeated adhesion strength of the hydrogels to various substrates; (f) adhesion mechanism between the hydrogel and various substrates.

adhere to a variety of substrates such as glass, plastic, rubber, paper, wood, metal, and polydimethylsiloxane (Figure 4a). From Figure 4b,c, it can be seen that the hydrogels can adhere to the skin tightly, and there is no residue after peeling. The main reasons for the adhesive property of hydrogels were the non-covalent bond interaction between specific functional groups in hydrogels and the surface of objects, such as hydrogen bond, metal−ligand complex, $\pi-\pi$ stacking, hydrophobic interaction, and so on (Figure 4f). The adhesion test device is shown in Figure S3c. The influence of SL content and Ca^{2+} content on adhesion strength is investigated in Figure S3a,b. It was obvious that the adhesion strength improved with the increase of SL content, which was because the enhanced SL content lead to the increase of catechol groups, the decrease in cross-linking density, and the enhancement of hydrogen bond formation with other substrates. However, with the increase of Ca^{2+} content, the adhesive strength decreased, because Ca^{2+} cross-linking lead to a reduction of the catechol groups.[53] Meanwhile, Ca^{2+} formed ionic coordination with −COOH, consuming the −COOH content, leading to the weakening of the interaction with the substrate surface. Furthermore, the increased cross-linking network inhibited the movement of the polymer chain at the adhesive interface. Figure 4d investigates the adhesion of the SL-Ca^{2+}/PAM hydrogel to different substrates. It can be seen that the adhesion strength of the four materials followed the order: wood > glass > stainless steel > PDMS. The adhesion of SL-Ca^{2+}/PAM hydrogel to wood was 50.6 kPa, and its high adhesion strength could be attributed to the rough porous structure and polyhydroxy structure of wood, which was conducive to the infiltration of hydrogel and hydrogen bond formation. Figure S6a shows a comparison of the adhesion of lignin-based hydrogels to glass as reported in the literatures, which shows SL-Ca^{2+}/PAM hydrogel's excellent adhesion ability. The SL-Ca^{2+}/PAM hydrogel also showed good repeatability and stability. After 5 consecutive peeling on different substrates, the hydrogel still maintained high adhesion (Figure 4e). In summary, the excellent adhesion properties of the hydrogel ensure the effectiveness of the device assembly process and the accuracy of human motion signal acquisition.

3.4. Electromechanical Properties of the SL-Ca^{2+}/PAM Hydrogels. SL contained Na^{+}, which also made the hydrogel conductive. However, due to its low content and the addition of more $CaCl_2$, it was mainly the addition of $CaCl_2$ that caused the hydrogel to be conductive.[54−56] Therefore, the SL-Ca^{2+}/PAM hydrogel had high electrical conductivity, which can be glued to the human skin as a flexible sensor to monitor human movement. As shown in Figure 5a, the small bulb was connected to the hydrogel to form a closed circuit. It can be seen that under the condition of no strain, the small bulb emitted bright light with a halo. When the hydrogel was stretched to 400% strain, the brightness of the small bulb dimmed, which was caused by the narrowing of the ion channel by stretching, and the resistance was increased. With the increase of Ca^{2+} concentration from 30 to 45 wt %, the conductivity decreased from 11.6 to 6.8 mS·cm^{-1} (Figure 5b).

https://doi.org/10.1021/acsomega.2c08097
ACS Omega 2023, 8, 9434−9444

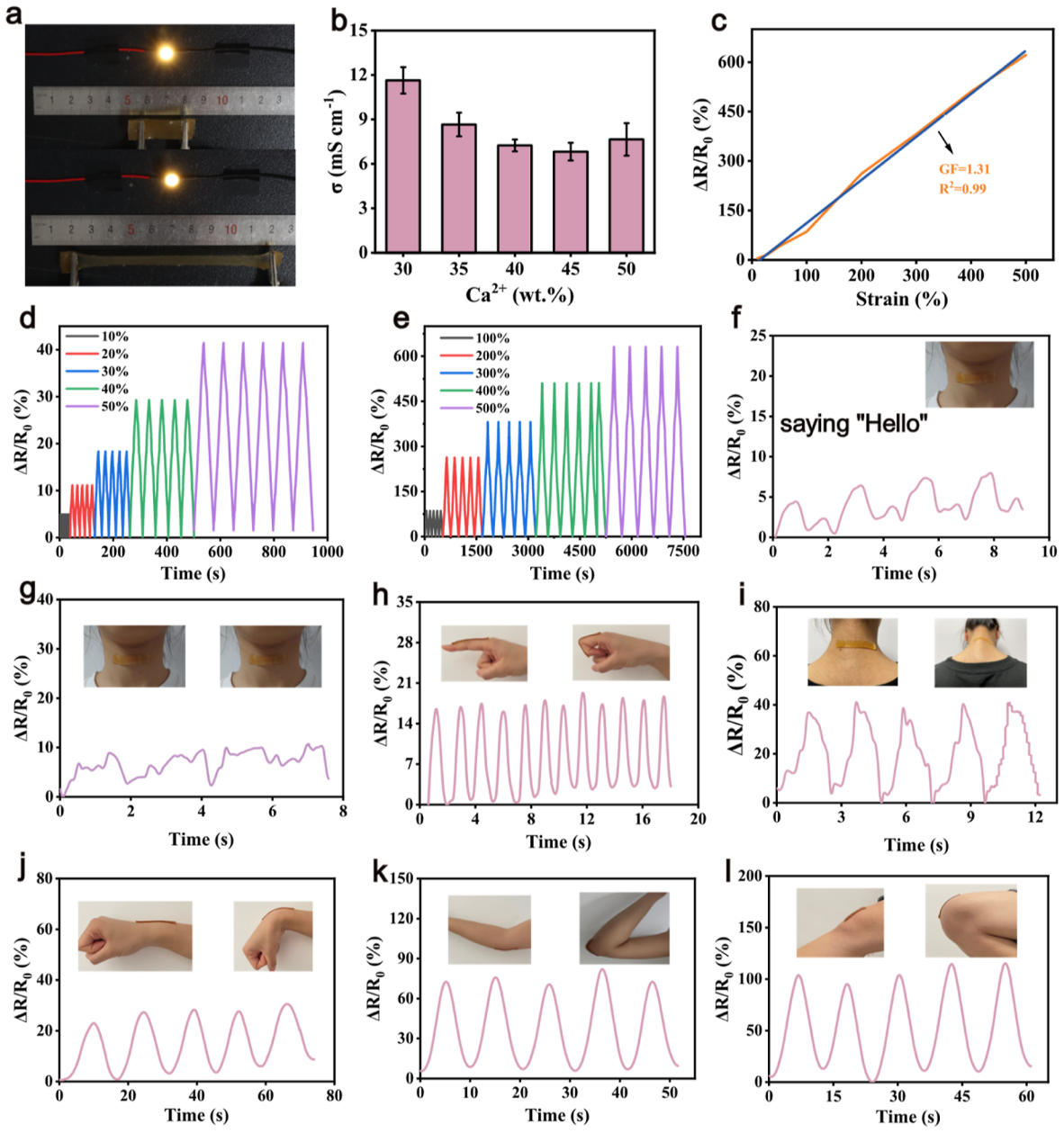

Figure 5. Sensing performance of the SL-Ca^{2+}/PAM hydrogel. (a) Luminance variation of the hydrogel at different elongations; (b) conductivity of the hydrogel with different calcium ion concentrations; (c) GF of the hydrogel in 500% strain range; (d) the relative resistance of the hydrogel varies from 10 to 50%; (e) the relative resistance of the hydrogel varies from 100 to 500%; detection of motions of (f) pronunciation of "Hello"; (g) swallowing; (h) finger; (i) neck nodding; (j) wrist; (k) elbow; and (l) knee.

This could be because with the increase of Ca^{2+}, it formed more coordination with −COOH, and the cross-linking density increased, leading the ion channel to narrow.[40] When the Ca^{2+} content reached 50 wt %, the conductivity increased slightly. Sensitivity (GF) is an important index of the sensor, defined as the ratio of the change of relative resistance to the applied strain. In Figure 5c, GF is 1.31 in a wide strain range of 0−500%, and there is a highly linear relationship between the relative resistance and strain (R^2 = 0.995). Stability and repeatability are also critical for sensors. Figure 5d,e shows the curves stretched five times under small strain (10−50%) and large strain (100−500%), and no significant deviation was observed in the resistance change rate, indicating that the hydrogel sensor had repeatability, stability, and a wide detection range. In order to observe the SL-Ca^{2+}/PAM hydrogel as a sensor for monitoring various human deformations, the hydrogel was cut into thin slices and adhered to different parts of the human body. The relative resistance curves can be observed as the sensor responds to motion in different parts of the body (Figure 5f−l). It can detect human movement in real time. In addition to detecting large movements, hydrogel sensors were sensitive enough to detect small movements. As shown in Figure 5f,g, when the throat made a swallowing motion and a sound, it could be seen that the change rate of the relative resistance reacted regularly with the action, which further indicated that the hydrogel sensor had good electrical stability and high sensitivity. The hydrogel sensor was also suitable for compressive strain. Figure S4a shows the electrical signals generated by pressing the cylindrical hydrogel, and Figure S4b shows the electrical signals

https://doi.org/10.1021/acsomega.2c08097
ACS Omega 2023, 8, 9434−9444

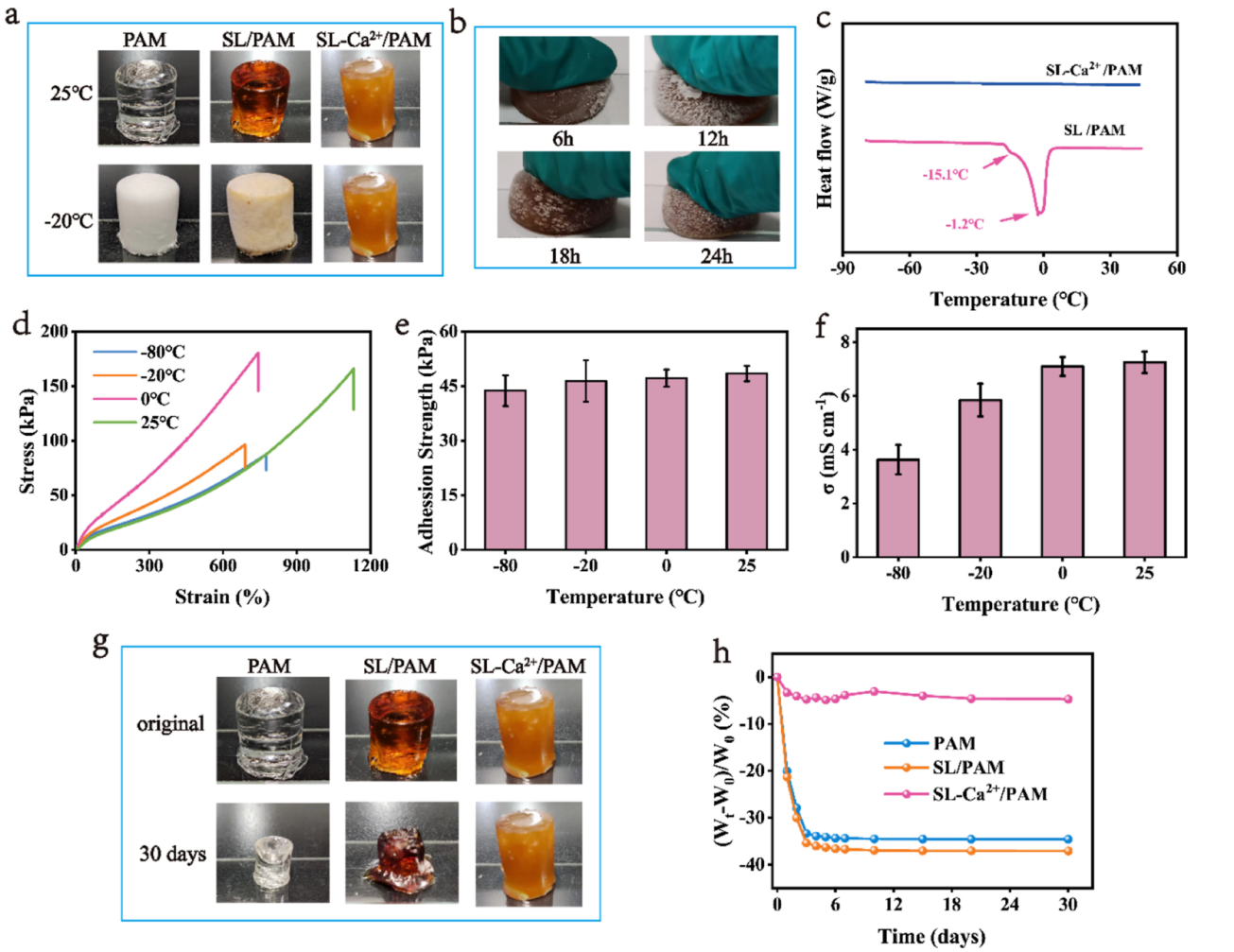

Figure 6. Anti-freezing and anti-dehydration properties of the SL-Ca^{2+}/PAM hydrogel; (a) comparison of PAM, SL/PAM, and SL-Ca^{2+}/PAM hydrogels before and after putting into −20 °C for 24 h; (b) comparison of SL-Ca^{2+}/PAM hydrogels placed at −80 °C at different times; (c) DSC curves of SL/PAM and SL-Ca^{2+}/PAM hydrogels; (d) tensile stress−strain curves of SL-Ca^{2+}/PAM hydrogels at different temperatures; (e) adhesion strength of SL-Ca^{2+}/PAM hydrogels to glass at different temperatures; (f) conductivity of SL-Ca^{2+}/PAM hydrogels at different temperatures; (g) comparison of the initial shape and morphology of PAM, SL/PAM, and SL-Ca^{2+}/PAM hydrogels after 30 days at room temperature; (h) relative changes of PAM, SL/PAM, and SL-Ca^{2+}/PAM hydrogels with time at room temperature.

generated by sticking the hydrogel to the foot and walking slowly. Therefore, SL-Ca^{2+}/PAM hydrogels have the characteristics of good stability, high sensitivity, and wide sensing range.

3.5. Anti-freezing and Anti-dehydration Properties of the SL-Ca^{2+}/PAM Hydrogels. Conventional hydrogels freeze at low temperatures or dehydrate at room temperature, which severely limit their applications as sensors. In this experiment, the hydrogel was given anti-freezing and anti-dehydration properties by adding $CaCl_2$, which can lower the freezing point the of aqueous phase, weaken the hydrogen bond inside the water molecules, destroy the aggregation of water molecules, and effectively hinder the formation of ice crystals in the hydrogel. Figure 6a shows the comparison of the SL-Ca^{2+}/PAM hydrogel, SL/PAM hydrogel, and PAM hydrogel placed at −20 °C for 24 h. It was clear that the SL/PAM hydrogel and PAM hydrogel without $CaCl_2$ were frozen solid, becoming both opaque and hard. In contrast, the SL-Ca^{2+}/PAM hydrogel still remained intact, soft, and tough. To study the low-temperature resistance of the SL-Ca^{2+}/PAM hydrogel, the shape was observed after being placed in an ultra-low temperature refrigerator at −80 °C for 6, 12, 18, and 24 h. As can be seen from Figure 6b, there was no change inside the hydrogel when it was left at −80 °C for 6 h, and few ice crystals were formed inside the hydrogel when it was left for 12 h. Indeed, even after 24 h, the hydrogel can also be pressed down completely, showing excellent anti-freezing property. In order to accurately investigate the finite freezing temperature of the hydrogel, DSC[57,58] was carried out from −80 °C to 50 °C. As shown in Figure 6c, the SL/PAM hydrogel had a sharp endothermic peak and a wide endothermic peak at −1.2 and −15.1 °C, corresponding to the melting point of free water and bound water, respectively. Notably, the SL-Ca^{2+}/PAM hydrogel did not appear endothermic peak, indicating that it did not produce ice crystals in the test temperature range. It is difficult for other anti-freezing gels to reach (Figure S6b). To better evaluate the application potential of hydrogels, the tensile properties, adhesion properties, and electrical conductivity of hydrogels were investigated at 0, −20, and −80 °C (Figure 6d−f). The tensile stress−strain curves illustrated that the mechanical properties of the hydrogels decreased at low temperatures but still maintained 87.5 kPa tensile strength and 775% stretching strain. This confirmed the outstanding flexibility of hydrogels at low temperatures. This was an unobvious change in the adhesion of the hydrogel to the glass

https://doi.org/10.1021/acsomega.2c08097
ACS Omega 2023, 8, 9434−9444

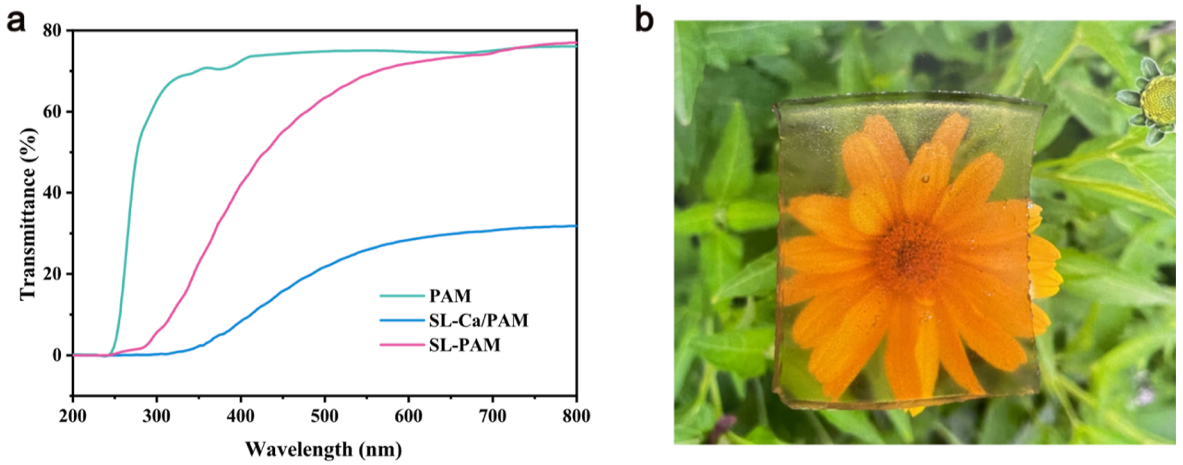

Figure 7. UV shielding performance of the SL-Ca^{2+}/PAM hydrogel. (a) UV−vis transmission spectrum of the PAM, SL/PAM, and SL-Ca^{2+}/PAM hydrogels; (b) high transparency image of the SL-Ca^{2+}/PAM hydrogel.

sheet in cold conditions and still reached 43.7 kPa, which meets the application of hydrogel electronics. Although the conductivity decreased with the reduced temperature, an ultrahigh ionic conductivity of 3.6 mS·cm^{-1} was also obtained at −80 °C, which ensured the feasibility of the SL-Ca^{2+}/PAM hydrogel application at low temperatures.

The dehydration of hydrogels is another challenge for flexible sensors. The SL-Ca^{2+}/PAM, SL/PAM, and PAM hydrogels were stored at room temperature of about 30 °C and relative humidity of about 80% for 30 days to investigate the water retention capacity of the hydrogels. As shown in Figure 6g, the SL/PAM hydrogels and PAM hydrogels were severely dehydrated and became particularly shriveled, while SL-Ca^{2+}/PAM hydrogels had little change after 30 days. The PAM hydrogel dropped to 65% of its initial weight, the SL/PAM hydrogel could only maintain 63% of its original mass, compared to the SL-Ca^{2+}/PAM hydrogel, which was still 94% of its weight (Figure 6h). This phenomenon can be attributed to the fact that the vapor pressure inside the hydrogel with $CaCl_2$ is lower than the ambient air pressure and that $CaCl_2$ has the ability to absorb water, thus making the hydrogel resistant to dehydration. In short, the anti-freezing and anti-dehydration ability of SL-Ca^{2+}/PAM hydrogel guarantees their use in extreme conditions.

3.6. UV-Shielding Performance of the SL-Ca^{2+}/PAM Hydrogels. Due to the polyphenol structure of SL, the hydrogels have UV shielding properties. In Figure 7a, at a wavelength of 365 nm, the transmittance of the PAM hydrogel was about 70.7%, and after adding SL, the transmittance was about 28.5%.[56] When Ca^{2+} was added again, the transmittance was only 3.6%. This was due to the reduced transparency of the hydrogel after the addition of Ca^{2+}, which blocked most UV rays. At the same time, the hydrogel was still visible. As shown in Figure 7b, after being covered by 2 mm hydrogel, the color and line of the flower can be clearly seen. The combination of UV-blocking and transparency allowed conductive hydrogels to significantly expand their applications in flexible sensors.

4. CONCLUSIONS

In summary, we report a rapid gelation strategy based on metal ion catalysis. Ca^{2+} can activate APS to produce free radicals and trigger environmental polymerization of AM monomers. Thanks to the covalent, hydrogen, and ionic coordination bonds of the hydrogel network, the resulting hydrogels had good mechanical properties (1153% elongation and tensile strength of 168 kPa), high electrical conductivity (7.2 mS·cm^{-1}), and excellent adhesion to different substrates given by the catechol group in SL; profiting from the physicochemical properties of $CaCl_2$, the hydrogels were endowed with anti-freezing and moisturizing properties, which can be maintained even at −80 °C. In addition, the hydrogels also exhibited excellent UV resistance (blocking UV by 95.1%) due to the polyphenolic structure of SL. SL-Ca^{2+}/PAM hydrogels were made into flexible skin sensors, which can sense small movements of swallow and speech and large movements of limbs such as wrists and knees. They have potential application prospects in flexible sensors. In short, this study opens up a broad prospect for hydrogel flexible electronics in extreme environments such as low temperatures and high-altitude areas.

■ ASSOCIATED CONTENT

Supporting Information

The Supporting Information is available free of charge at https://pubs.acs.org/doi/10.1021/acsomega.2c08097.

Hydrogel formula lists; comparison table of tensile mechanics; stress and strain curves of AM and MBA variables; EDS image; adhesion strength of different SL and Ca^{2+} contents; attached device; pressure sensor; effect of SL content and Ca^{2+} content on gelation time; and comparison of adhesion strength and freezing point (PDF)

■ AUTHOR INFORMATION

Corresponding Author

Jiufang Duan − *MOE Engineering Research Center of Forestry Biomass Materials and Bioenergy, Beijing Forestry University, Beijing 100083, China;* orcid.org/0000-0002-1310-1404; Email: duanjiu99@163.com

Authors

Hui Lv − *MOE Engineering Research Center of Forestry Biomass Materials and Bioenergy, Beijing Forestry University, Beijing 100083, China;* orcid.org/0000-0002-9480-5322

https://doi.org/10.1021/acsomega.2c08097
ACS Omega 2023, 8, 9434−9444

Shiyu Zong − *MOE Engineering Research Center of Forestry Biomass Materials and Bioenergy, Beijing Forestry University, Beijing 100083, China*
Tong Li − *MOE Engineering Research Center of Forestry Biomass Materials and Bioenergy, Beijing Forestry University, Beijing 100083, China*
Qian Zhao − *MOE Engineering Research Center of Forestry Biomass Materials and Bioenergy, Beijing Forestry University, Beijing 100083, China*
Zhiyong Xu − *MOE Engineering Research Center of Forestry Biomass Materials and Bioenergy, Beijing Forestry University, Beijing 100083, China*

Complete contact information is available at: https://pubs.acs.org/10.1021/acsomega.2c08097

Notes

The authors declare no competing financial interest.

■ ACKNOWLEDGMENTS

This research was supported by the National Key Research and Development Program of China (2022YFD2200804-4), and the National Natural Science Foundation of China (31600464).

■ REFERENCES

(1) Liu, J.; Khanam, Z.; Ahmed, S.; Wang, H.; Wang, T.; Song, S. A study of low-temperature solid-state supercapacitors based on Al-ion conducting polymer electrolyte and graphene electrodes. *J. Power Sources* **2021**, *488*, 229461.
(2) Xu, T.; Liu, K.; Sheng, N.; Zhang, M.; Liu, W.; Liu, H.; Dai, L.; Zhang, X.; Si, C.; Du, H.; et al. Biopolymer-based hydrogel electrolytes for advanced energy storage/conversion devices: Properties, applications, and perspectives. *Energy Storage Mater.* **2022**, *48*, 244−262.
(3) Wen, J.; Tang, J.; Ning, H.; Hu, N.; Zhu, Y.; Gong, Y.; Xu, C.; Zhao, Q.; Jiang, X.; Hu, X.; et al. Multifunctional Ionic Skin with Sensing, UV-Filtering, Water-Retaining, and Anti-Freezing Capabilities. *Adv. Funct. Mater.* **2021**, *31*, 2011176.
(4) Ba, Y.-Y.; Bao, J.-F.; Liu, X.-T.; Li, X.-W.; Deng, H.-T.; Wen, D.-l.; Zhang, X.-S. Electron-Ion Coupling Mechanism to Construct Stable Output Performance Nanogenerator. *Research* **2021**, *2021*, 9817062.
(5) Ying, B.; Zuo, R.; Wan, Y.; Liu, X. An Ionic Hydrogel-Based Antifreezing Triboelectric Nanogenerator. *ACS Appl. Electron. Mater.* **2022**, *4*, 1930−1938.
(6) Liu, X.-W.; Huang, Y.-X.; Sun, X.-F.; Sheng, G.-P.; Zhao, F.; Wang, S.-G.; Yu, H.-Q. Conductive Carbon Nanotube Hydrogel as a Bioanode for Enhanced Microbial Electrocatalysis. *ACS Appl. Mater. Interfaces* **2014**, *6*, 8158−8164.
(7) Pan, Z.; Wang, Z.-Y.; Wang, M.-H.; Yang, L.; Yu, S.-H. Adhesive aero-hydrogel hybrid conductor assembled from silver nanowire architectures. *Sci. China Mater.* **2021**, *64*, 2868−2876.
(8) Xiong, Z.-C.; Yang, Z.-Y.; Zhu, Y.-J.; Chen, F.-F.; Zhang, Y.-G.; Yang, R.-L. Ultralong Hydroxyapatite Nanowires-Based Paper Co-Loaded with Silver Nanoparticles and Antibiotic for Long-Term Antibacterial Benefit. *ACS Appl. Mater. Interfaces* **2017**, *9*, 22212−22222.
(9) Li, Y.; Li, C.; Zhao, S.; Cui, J.; Zhang, G.; Gao, A.; Yan, Y. Facile fabrication of highly conductive and robust three-dimensional graphene/silver nanowires bicontinuous skeletons for electromagnetic interference shielding silicone rubber nanocomposites. *Compos. - A: Appl. Sci. Manuf.* **2019**, *119*, 101−110.
(10) Liu, H.; Xu, T.; Cai, C.; Liu, K.; Liu, W.; Zhang, M.; Du, H.; Si, C.; Zhang, K. Multifunctional Superelastic, Superhydrophilic, and Ultralight Nanocellulose-Based Composite Carbon Aerogels for Compressive Supercapacitor and Strain Sensor. *Adv. Funct. Mater.* **2022**, *32*, 2113082.
(11) Yue, Z.; Zhu, Y.; Xia, J.; Wang, Y.; Ye, X.; Jiang, H.; Jia, H.; Lin, Y.; Jia, C. Sponge Graphene Aerogel Pressure Sensors with an Extremely Wide Operation Range for Human Recognition and Motion Detection. *ACS Appl. Electron. Mater.* **2021**, *3*, 1301−1310.
(12) Lee, K. H.; Zhang, Y.-Z.; Kim, H.; Lei, Y.; Hong, S.; Wustoni, S.; Hama, A.; Inal, S.; Alshareef, H. N. Muscle Fatigue Sensor Based on Ti 3 C 2 T x MXene Hydrogel. *Small Methods* **2021**, *5*, 2100819.
(13) Chen, Y.; Fu, X.; Kang, S.; Wang, L.; Lu, W. Strategy of Fabricating Flexible Strain Sensor via Layer-by-Layer Assembly of Conductive Hydrogels. *ACS Appl. Electron. Mater.* **2021**, *3*, 3889−3897.
(14) Zhang, L.; Wu, Y.; Xia, Y.; Jin, L. High capacitance of polypyrrole hydrogel electrode synthesized by polymerization of conjugated pyrrole salt. *Electrochim. Acta* **2022**, *412*, 140108.
(15) Duan, J.; Wen, H.; Zong, S.; Li, T.; Lv, H.; Liu, L. Soft/Hard Controllable Conversion Galactomannan Ionic Conductive Hydrogel as a Flexible Sensor. *ACS Appl. Electron. Mater.* **2021**, *3*, 5000−5014.
(16) Han, L.; Lu, X.; Liu, K.; Wang, K.; Fang, L.; Weng, L.-T.; Zhang, H.; Tang, Y.; Ren, F.; Zhao, C.; et al. Mussel-Inspired Adhesive and Tough Hydrogel Based on Nanoclay Confined Dopamine Polymerization. *ACS Nano* **2017**, *11*, 2561−2574.
(17) Kong, L.; Gao, Z.; Li, X.; Gao, G. An amylopectin-enabled skin-mounted hydrogel wearable sensor. *J. Mater. Chem. B* **2021**, *9*, 1082−1088.
(18) Xu, J.; Jin, R.; Duan, L.; Ren, X.; Gao, G. Tough, adhesive and conductive polysaccharide hydrogels mediated by ferric solution. *Carbohydr. Polym.* **2019**, *211*, 1−10.
(19) Wang, G.; Zhang, Q.; Wang, Q.; Zhou, L.; Gao, G. Bio-Based Hydrogel Transducer for Measuring Human Motion with Stable Adhesion and Ultrahigh Toughness. *ACS Appl. Mater. Interfaces* **2021**, *13*, 24173−24182.
(20) Liu, X.; Zhang, Q.; Gao, G. Bioinspired Adhesive Hydrogels Tackified by Nucleobases. *Adv. Funct. Mater.* **2017**, *27*, 1703132.
(21) Yan, J.; Ji, Y.; Huang, M.; Li, T.; Liu, Y.; Lü, S.; Liu, M. Nucleobase-Inspired Self-Adhesive and Inherently Antibacterial Hydrogel for Wound Dressing. *ACS Mater. Lett.* **2020**, *2*, 1375−1380.
(22) Zhang, X.; Cui, C.; Chen, S.; Meng, L.; Zhao, H.; Xu, F.; Yang, J. Adhesive Ionohydrogels Based on Ionic Liquid/Water Binary Solvents with Freezing Tolerance for Flexible Ionotronic Devices. *Chem. Mater.* **2022**, *34*, 1065−1077.
(23) Hao, S.; Shao, C.; Meng, L.; Cui, C.; Xu, F.; Yang, J. Tannic Acid-Silver Dual Catalysis Induced Rapid Polymerization of Conductive Hydrogel Sensors with Excellent Stretchability, Self-Adhesion, and Strain-Sensitivity Properties. *ACS Appl. Mater. Interfaces* **2020**, *12*, 56509−56521.
(24) Quan, W.-Y.; Hu, Z.; Liu, H.-Z.; Ouyang, Q.-Q.; Zhang, D.-Y.; Li, S.-D.; Li, P.-W.; Yang, Z.-M. Mussel-Inspired Catechol-Functionalized Hydrogels and Their Medical Applications. *Molecules* **2019**, *24*, 2586.
(25) Ahn, B. K. Perspectives on Mussel-Inspired Wet Adhesion. *J. Am. Chem. Soc.* **2017**, *139*, 10166−10171.
(26) Han, L.; Liu, K.; Wang, M.; Wang, K.; Fang, L.; Chen, H.; Zhou, J.; Lu, X. Mussel-Inspired Adhesive and Conductive Hydrogel with Long-Lasting Moisture and Extreme Temperature Tolerance. *Adv. Funct. Mater.* **2018**, *28*, 1704195.
(27) Wang, M.; Zhang, P.; Shamsi, M.; Thelen, J. L.; Qian, W.; Truong, T.; Ma, J.; Hu, J.; Dickey, M. D. Tough and stretchable ionogels by in situ phase separation. *Nat. Mater.* **2022**, *21*, 359−365.
(28) Meng, Y.; Lu, J.; Cheng, Y.; Li, Q.; Wang, H. Lignin-based hydrogels: A review of preparation, properties, and application. *Int. J. Biol. Macromol.* **2019**, *135*, 1006−1019.
(29) Liu, H.; Xu, T.; Liu, K.; Zhang, M.; Liu, W.; Li, H.; Du, H.; Si, C. Lignin-based electrodes for energy storage application. *Ind. Crops Prod.* **2021**, *165*, 113425.
(30) Lee, Y.-Y.; Kang, H.-Y.; Gwon, S. H.; Choi, G. M.; Lim, S.-M.; Sun, J.-Y.; Joo, Y.-C. A Strain-Insensitive Stretchable Electronic

Conductor: PEDOT:PSS/Acrylamide Organogels. *Adv. Mater.* **2016**, *28*, 1636−1643.
(31) Zhang, X.; Wang, K.; Hu, J.; Zhang, Y.; Dai, Y.; Xia, F. Role of a high calcium ion content in extending the properties of alginate dual-crosslinked hydrogels. *J. Mater. Chem. A* **2020**, *8*, 25390−25401.
(32) Ma, S.; Yan, C.; Cai, M.; Yang, J.; Wang, X.; Zhou, F.; Liu, W. Continuous Surface Polymerization via Fe(II)-Mediated Redox Reaction for Thick Hydrogel Coatings on Versatile Substrates. *Adv. Mater.* **2018**, *30*, 1803371.
(33) Zhang, X.-F.; Ma, X.; Hou, T.; Guo, K.; Yin, J.; Wang, Z.; Shu, L.; He, M.; Yao, J. Inorganic Salts Induce Thermally Reversible and Anti-Freezing Cellulose Hydrogels. *Angew. Chem. Int. Ed.* **2019**, *58*, 7366−7370.
(34) Jia, Z.; Zeng, Y.; Tang, P.; Gan, D.; Xing, W.; Hou, Y.; Wang, K.; Xie, C.; Lu, X. Conductive, Tough, Transparent, and Self-Healing Hydrogels Based on Catechol-Metal Ion Dual Self-Catalysis. *Chem. Mater.* **2019**, *31*, 5625−5632.
(35) Jie, J.; Kongyin, K.; Xinxin, X.; Zhijiang, Z.; Min, M.; Tian, T.; Junfu, J. Preparation and characterization of carboxyl multi-walled carbon nanotubes/calcium alginate composite hydrogel nano-filtration membrane. *Mater. Lett.* **2015**, *157*, 112−115.
(36) Gao, F.; Zhang, Y.; Li, Y.; Xu, B.; Cao, Z.; Liu, W. Sea Cucumber-Inspired Autolytic Hydrogels Exhibiting Tunable High Mechanical Performances, Repairability, and Reusability. *ACS Appl. Mater. Interfaces* **2016**, *8*, 8956−8966.
(37) Li, N.; Sun, D.; Su, Z.; Hao, X.; Li, M.; Ren, J.; Peng, F. Rapid fabrication of xylan-based hydrogel by graft polymerization via a dynamic lignin-Fe3+ plant catechol system. *Carbohydr. Polym.* **2021**, *269*, 118306.
(38) Du, L.; Cao, S.; Zheng, X.; Jiang, L.; Ren, Z.; Chen, J.; Xu, Q. Superfast Self-Healing and Photothermal Active Hydrogel with Nondefective Graphene as Effective Additive. *Macromol. Mater. Eng.* **2020**, *305*, 2000172.
(39) Huang, Y.; Liu, J.; Wang, J.; Hu, M.; Mo, F.; Liang, G.; Zhi, C. An Intrinsically Self-Healing NiCo||Zn Rechargeable Battery with a Self-Healable Ferric-Ion-Crosslinking Sodium Polyacrylate Hydrogel Electrolyte. *Angew. Chem. Int. Ed.* **2018**, *57*, 9810−9813.
(40) Zhao, H.; Hao, S.; Fu, Q.; Zhang, X.; Meng, L.; Xu, F.; Yang, J. Ultrafast Fabrication of Lignin-Encapsulated Silica Nanoparticles Reinforced Conductive Hydrogels with High Elasticity and Self-Adhesion for Strain Sensors. *Chem. Mater.* **2022**, *34*, 5258−5272.
(41) Fu, Q.; Hao, S.; Meng, L.; Xu, F.; Yang, J. Engineering Self-Adhesive Polyzwitterionic Hydrogel Electrolytes for Flexible Zinc-Ion Hybrid Capacitors with Superior Low-Temperature Adaptability. *ACS Nano* **2021**, *15*, 18469−18482.
(42) Xu, H.; Nishida, J.; Ma, W.; Wu, H.; Kobayashi, M.; Otsuka, H.; Takahara, A. Competition between Oxidation and Coordination in Cross-Linking of Polystyrene Copolymer Containing Catechol Groups. *ACS Macro Lett.* **2012**, *1*, 457−460.
(43) Gan, D.; Xing, W.; Jiang, L.; Fang, J.; Zhao, C.; Ren, F.; Fang, L.; Wang, K.; Lu, X. Plant-inspired adhesive and tough hydrogel based on Ag-Lignin nanoparticles-triggered dynamic redox catechol chemistry. *Nat. Commun.* **2019**, *10*, 1487.
(44) Wang, Q.; Guo, J.; Lu, X.; Ma, X.; Cao, S.; Pan, X.; Ni, Y. Wearable lignin-based hydrogel electronics: A mini-review. *Int. J. Biol. Macromol.* **2021**, *181*, 45−50.
(45) Xiu, H.; Zhao, H.; Dai, L.; Li, J.; Wang, Z.; Cui, Y.; Bai, Y.; Zheng, X.; Li, J. Robust and adhesive lignin hybrid hydrogel as an ultrasensitive sensor. *Int. J. Biol. Macromol.* **2022**, *213*, 226−233.
(46) Wang, H.; Li, Z.; Zuo, M.; Zeng, X.; Tang, X.; Sun, Y.; Lin, L. Stretchable, freezing-tolerant conductive hydrogel for wearable electronics reinforced by cellulose nanocrystals toward multiple hydrogen bonding. *Carbohydr. Polym.* **2022**, *280*, 119018.
(47) Yan, G.; He, S.; Ma, S.; Zeng, A.; Chen, G.; Tang, X.; Sun, Y.; Xu, F.; Zeng, X.; Lin, L. Catechol-based all-wood hydrogels with anisotropic, tough, and flexible properties for highly sensitive pressure sensing. *Chem. Eng. J.* **2022**, *427*, 131896.
(48) Zhu, Y.; Lin, L.; Chen, Y.; Song, Y.; Lu, W.; Guo, Y. Extreme Temperature-Tolerant Conductive Gel with Antibacterial Activity for Flexible Dual-Response Sensors. *ACS Appl. Mater. Interfaces* **2020**, *12*, 56470−56479.
(49) Gao, Y.; Peng, J.; Zhou, M.; Yang, Y.; Wang, X.; Wang, J.; Cao, Y.; Wang, W.; Wu, D. A multi-model, large range and anti-freezing sensor based on a multi-crosslinked poly(vinyl alcohol) hydrogel for human-motion monitoring. *J. Mater. Chem. B* **2020**, *8*, 11010−11020.
(50) Liang, Q.; Xia, X.; Sun, X.; Yu, D.; Huang, X.; Han, G.; Mugo, S. M.; Chen, W.; Zhang, Q. Highly Stretchable Hydrogels as Wearable and Implantable Sensors for Recording Physiological and Brain Neural Signals. *Adv. Sci.* **2022**, *9*, 2201059.
(51) Jia, Z.; Lv, X.; Hou, Y.; Wang, K.; Ren, F.; Xu, D.; Wang, Q.; Fan, K.; Xie, C.; Lu, X. Mussel-inspired nanozyme catalyzed conductive and self-setting hydrogel for adhesive and antibacterial bioelectronics. *Bioact. Mater.* **2021**, *6*, 2676−2687.
(52) Sun, P.; Wang, J.; Yao, X.; Peng, Y.; Tu, X.; Du, P.; Zheng, Z.; Wang, X. Facile Preparation of Mussel-Inspired Polyurethane Hydrogel and Its Rapid Curing Behavior. *ACS Appl. Mater. Interfaces* **2014**, *6*, 12495−12504.
(53) Gong, X.; Fu, C.; Alam, N.; Ni, Y.; Chen, L.; Huang, L.; Hu, H.-C. Tannic acid modified hemicellulose nanoparticle reinforced ionic hydrogels with multi-functions for human motion strain sensor applications. *Ind. Crops Prod.* **2022**, *176*, 114412.
(54) Fu, C.; Liu, X.; Yi, Y.; Fatehi, P.; Meng, X.; Kong, F.; Wang, S. Lignin derived hydrogel with highly adhesive for flexible strain sensors. *Polym. Test.* **2022**, *107*, 107486.
(55) Sun, D.; Li, N.; Rao, J.; Jia, S. Y.; Su, Z. H.; Hao, X.; Peng, F. Ultrafast fabrication of organohydrogels with UV-blocking, anti-freezing, anti-drying, and skin epidermal sensing properties using lignin-Cu2+ plant catechol chemistry. *J. Mater. Chem. A* **2021**, *9*, 14381−14391.
(56) Wang, Q.; Pan, X.; Lin, C.; Ma, X.; Cao, S.; Ni, Y. Ultrafast gelling using sulfonated lignin-Fe3+ chelates to produce dynamic crosslinked hydrogel/coating with charming stretchable, conductive, self-healing, and ultraviolet-blocking properties. *Chem. Eng. J.* **2020**, *396*, 125341.
(57) Wang, Y.; Pang, B.; Wang, R.; Gao, Y.; Liu, Y.; Gao, C. An anti-freezing wearable strain sensor based on nanoarchitectonics with a highly stretchable, tough, anti-fatigue and fast self-healing composite hydrogel. *Compos. - A: Appl. Sci. Manuf.* **2022**, *160*, 107039.
(58) Yang, Y.; Yang, Y.; Cao, Y.; Wang, X.; Chen, Y.; Liu, H.; Gao, Y.; Wang, J.; Liu, C.; Wang, W.; et al. Anti-freezing, resilient and tough hydrogels for sensitive and large-range strain and pressure sensors. *Chem. Eng. J.* **2021**, *403*, 126431.

https://doi.org/10.1021/acsomega.2c08097
ACS Omega 2023, 8, 9434−9444